doi:10.1038/nature12374

1. Ice Sheet Model for Integrated Earth System Studies (IcIES-MIROC) (see Methods)

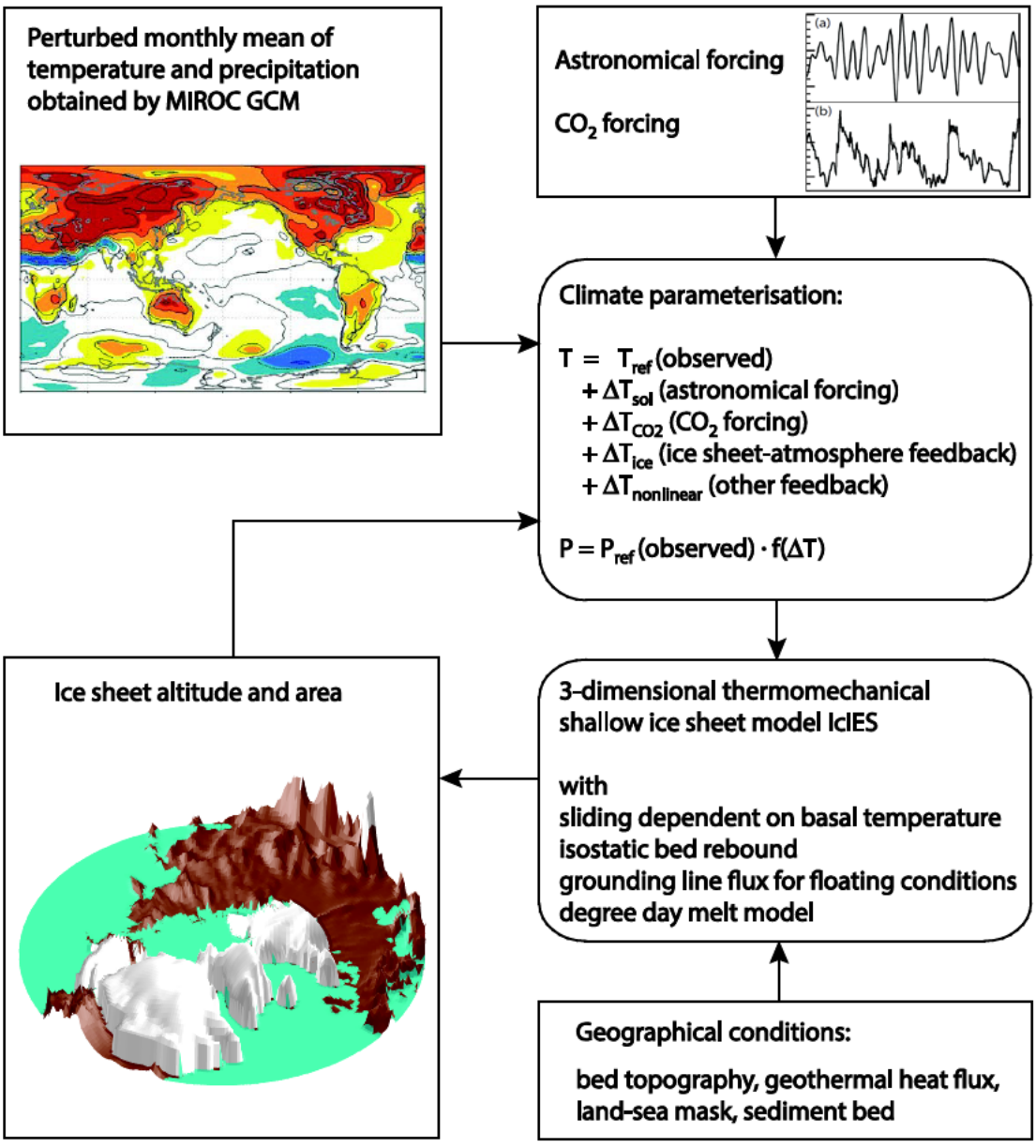

Fig. S1. Schematic representation of the IcIES-MIROC.

2. Simulated ice sheet cycles (variable atmospheric CO_2 content)

The modelled time series of ice volumes for a range of various model parameters, forced with the summer insolation at 65° north given by the variable astronomical parameters and reconstructed atmospheric CO_2 content, lie mostly within the scatter ranges of the reconstructed ice volumes[42-45]. Some deviations, especially the insufficient deglaciation in the Holocene, may be the result of missing processes in the model, such as a missing marine ice sheet physics with a potential for instability [46] for the Arctic Archipelago and the continental shelves of Barents and Kara Sea region, and uncertain calving parameterization. The simulated ice extent and retreat pattern of major Northern Hemisphere ice sheets are comparable to the reconstructions[47-49], although some deviations, especially in Scandinavia, may be due to the missing ocean circulation change and insufficient representation of orographic precipitation.

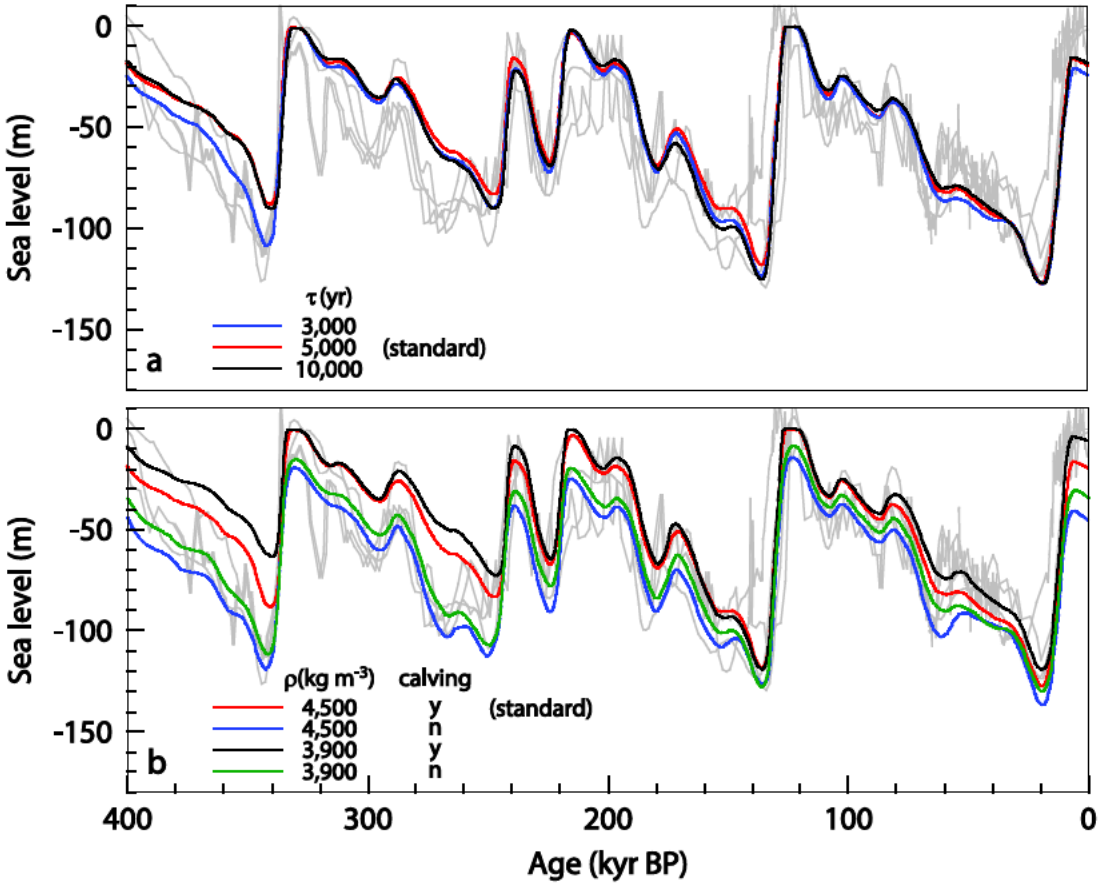

Figure S2. Dependence on model parameters of calving and isostasy with constant atmospheric CO_2 content. Simulated evolution of the total Northern Hemisphere ice sheet volume during the last four glacial cycles, with and without the parameterization of active calving into proglacial lakes, with three different time constants) and for two different mantle densities for isostatic rebound. The model was forced with the Milankovitch forcing of the northern summer insolation with and without reconstructed atmospheric CO_2 variations. Different ice volume reconstructions showing the sensitivity of the model to three model parameters, time constant and mantle density for isostatic rebound and calving into proglacial lakes. **a**, Three different values for time constant, **b**, two different mantle densities with and without calving. The black lines in both panels show the standard case.

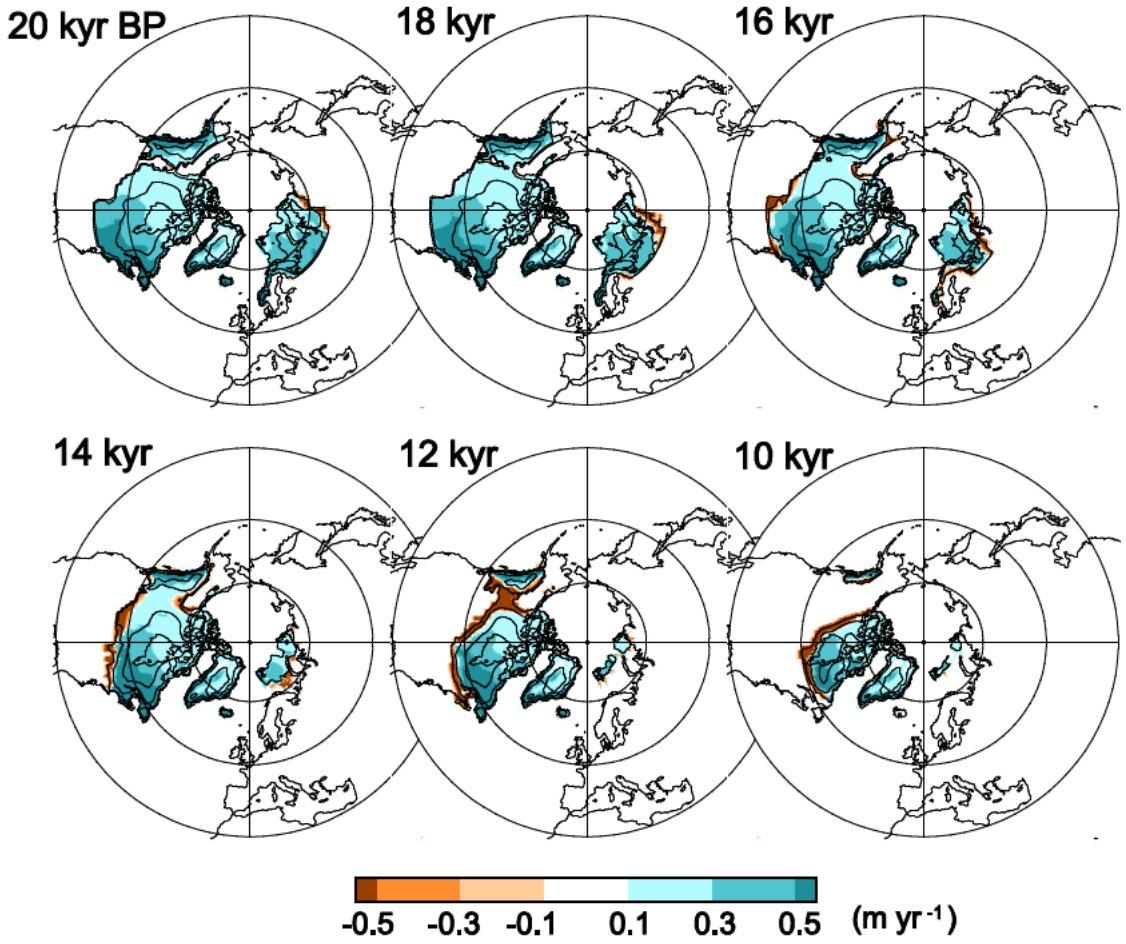

Figure S3. Simulated deglaciation from 20 to 10 kyr. Maps of altitude and surface mass balance of the Northern Hemisphere ice sheets at 20, 18, 16, 14, 12 and 10 kyr BP for the standard run (Fig. 1d), which corresponds to the transient ice volume evolution in Fig. 2b. Between 20 and 18 kyr, the mass balance of the North American ice sheet is strongly positive, corresponding to a situation in the blue area below the lower branch of the hysteresis loop (Fig. 2b). At 16 kyr, the mass balance comes close to neutral, and after crossing the upper hysteresis branch, it becomes strongly negative at 14, 12 and 10 kyr. Note that the extended areas of substantial melt in the low latitude started to develop shortly before crossing the upper hysteresis branch around 16 kyr BP.

3. Simulated ice sheet cycles (constant CO_2 content at 220 ppm)

The modelled time series of ice volumes for a range of model parameters, forced with the summer insolation at 65° north given by the variable astronomical parameters and constant atmospheric CO_2 content still show the same periodicities as for the result with reconstructed CO_2 content.

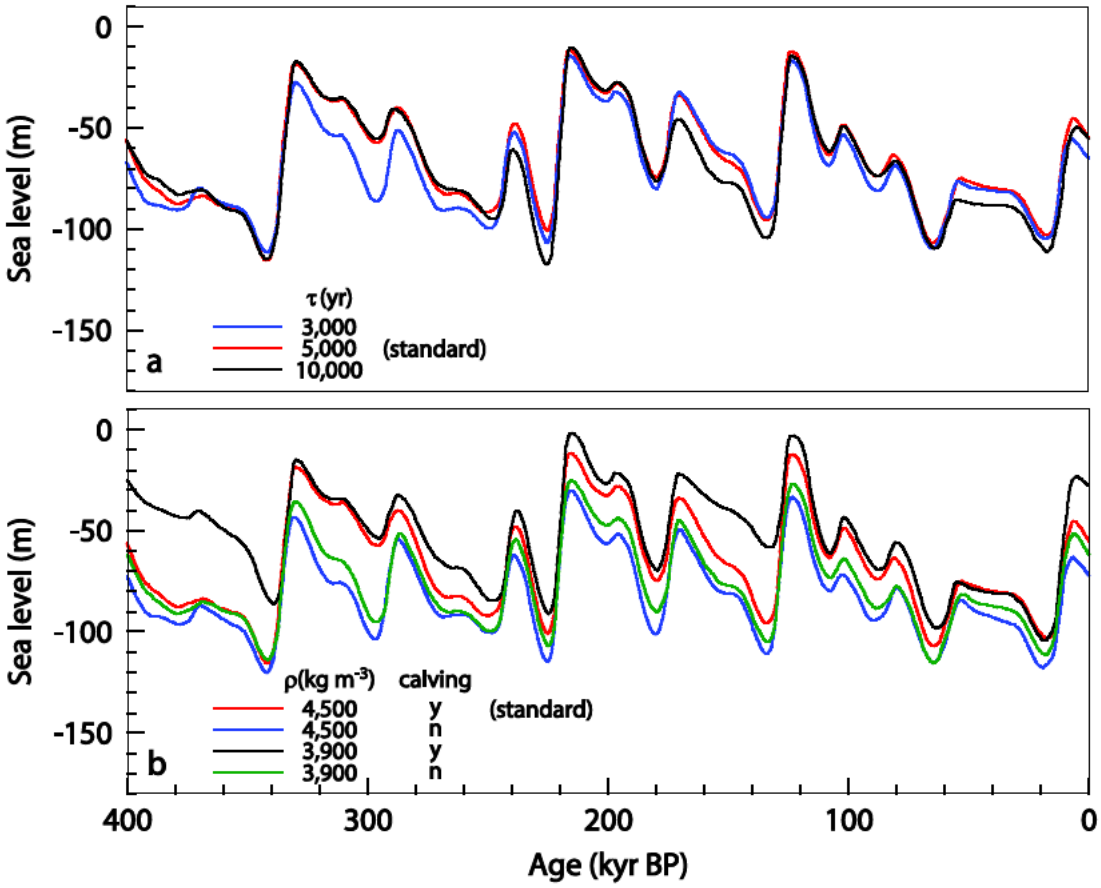

Figure S4. Role of calving, isostasy with variable reconstructed atmospheric CO_2 content. Simulated evolution of the total Northern Hemisphere ice sheet volume during the last four glacial cycles, with and without calving into proglacial lakes, with three different time constants and for two different mantle densities for isostatic rebound. The model was forced with the northern summer insolation with the Milankovitch forcing of the northern summer insolation and with constant atmospheric CO_2 at 220 ppm. Different ice volume reconstructions showing the sensitivity of the model to three model parameters, time constant and mantle density for isostatic rebound and calving into proglacial lakes. upper panel: three different values for time constant; lower panel: two different mantle densities with and without calving.

4. Influence of the initial conditions

To study the influence of the initial conditions on the model runs, we conducted experiments for 400-kyr periods starting from two different initial conditions. The initial conditions only influence the solution in the early part of the first 100-kyr cycle of the spin up run and they are mostly forgotten after the first deglaciation and interglacial period. The initial conditions of the 400-kyr experiments shown in this work stem from a transient spin up experiment for a 400-kyr period, with the same experimental setup for both 400-kyr periods.

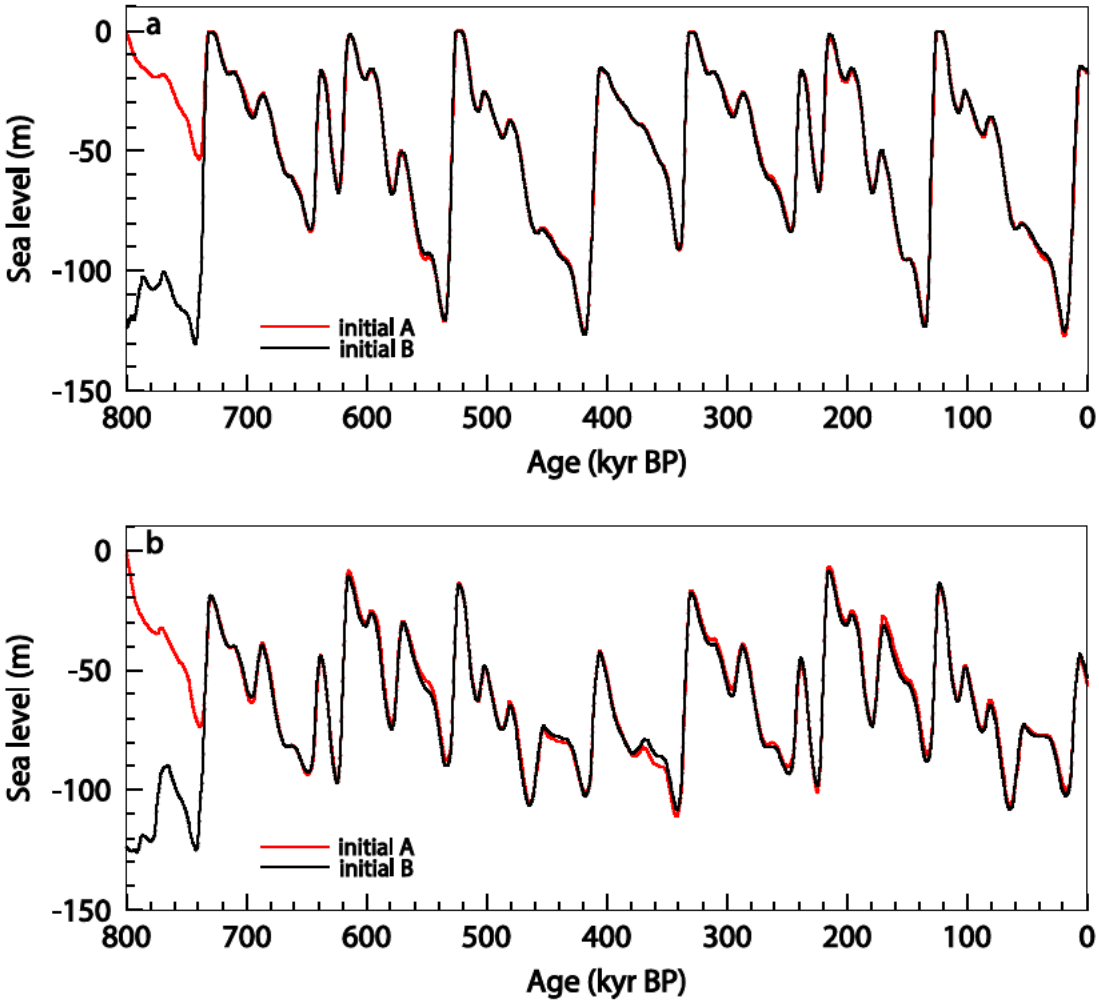

Fig. S5. Dependence of modeled glacial cycles on initial conditions of initial conditions. a, Evolution of ice volume in sea level equivalent with two different initial conditions. The insolation forcing corresponds to the Milankovitch forcing and the prescribed atmospheric content of CO_2 corresponds to the reconstructed CO_2 content of the past 400 kyr for both consequtive 400-kyr periods (-800 to -400 kyr and -400 to 0 kyr in the figure). The initial condition A corresponds to no ice condition and the initial condition B to an ice volume corresponding to a sea level change of 125 m. **b,** same as (**a**) but with constant atmospheric CO_2 content at 220 ppm.

5. Role of the various astronomical parameters

The simulated time series for ice volume only show ~100-kyr, ~40-kyr and ~20-kyr cycles if all astronomical parameters are variable. If one of the astronomical parameters is kept constant at a given value, ~100-kyr cycles remain only for a constant intermediate obliquitiy of 23.5°.

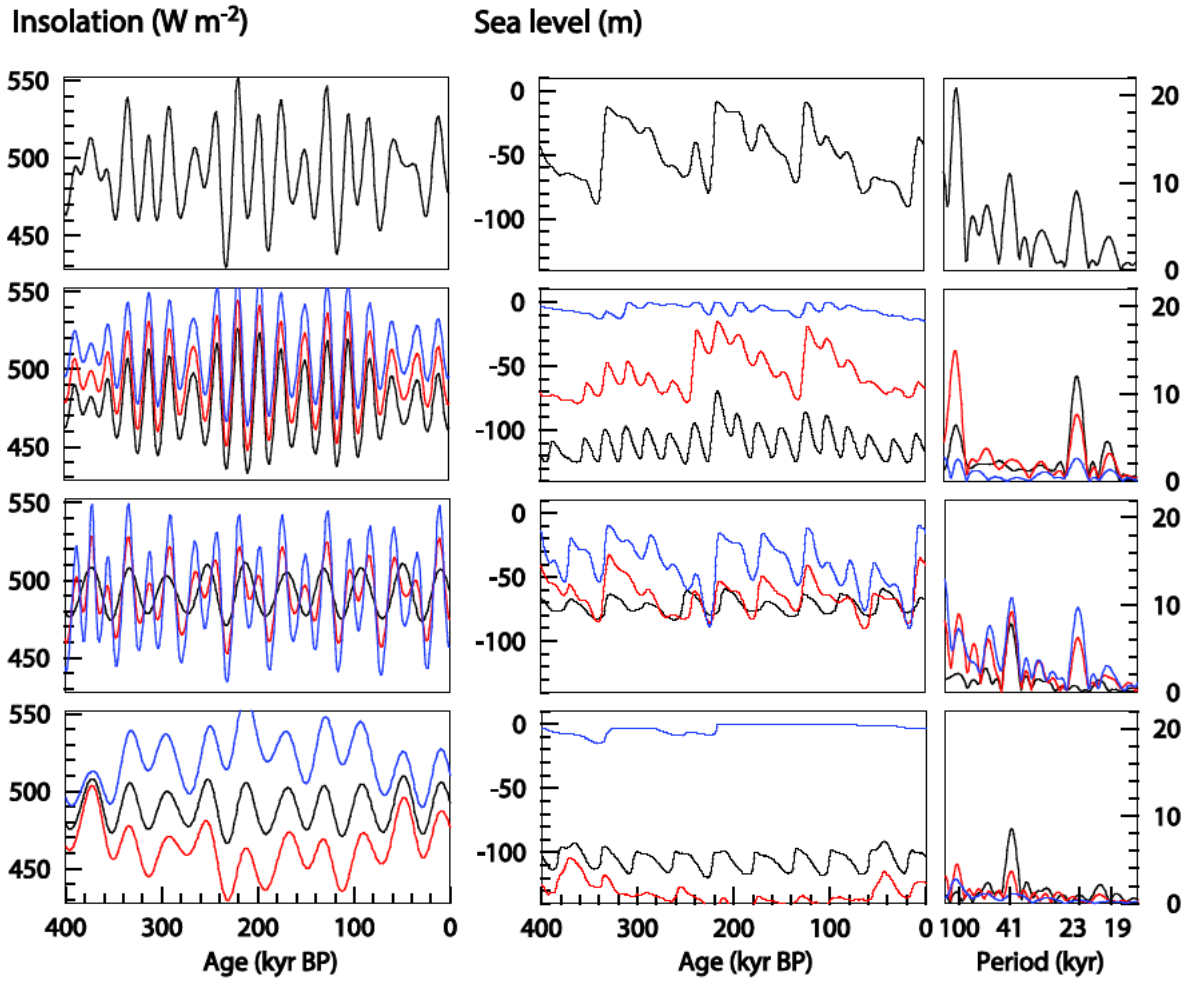

Figure S6. Role of the astronomical parameters in the 100 kyr cycles. Time series for the last four glacial cycles: north summer insolation forcing at 65° north (left side panels), modeled ice volume of the North American ice sheet for a constant CO_2 level of 220 ppm (middle panels), corresponding spectra (right panels). (top row) With all astronomical parameters varying, (second row) with constant obliquity of 22.5° (blue), 23.5° (red) and 24.5° (black), (third row) with constant eccentricity at 0.0 (black), 0.02 (red) and 0.04 (blue), (fourth row) with constant perihelion passage near north winter solstice (red), spring equinox (black) and summer solstice (blue).

References

42 Bintanja, R. & van de Wal, R. S. W. North American ice-sheet dynamics and the onset of 100,000-year glacial cycles. Nature 454, doi:10.1038/nature07158 (2008).

43 Siddall, M. et al. Sea-level fluctuations during the last glacial cycle. Nature 423, 853-858, doi:10.1038/nature01690 (2003).

44 Waelbroeck, C. et al. Sea-level and deep water temperature changes derived from benthic foraminifera isotopic records. Quaternary Science Reviews 21, 295-305, doi:10.1016/s0277-3791(01)00101-9 (2002).

45 Rohling, E. et al. Antarctic temperature and global sea level closely coupled over the past five glacial cycles. Nature Geoscience, 500-504, doi:DOI 10.1038/ngeo557 (2009).

46 Pattyn, F. et al. Results of the Marine Ice Sheet Model Intercomparison Project, MISMIP. Cryosphere 6, 573-588, doi:10.5194/tc-6-573-2012 (2012).

47 Dyke, A. S. et al. The Laurentide and Innuitian ice sheets during the Last Glacial Maximum. Quaternary Science Reviews 21, 9-31, doi:10.1016/s0277-3791(01)00095-6 (2002).

48 Peltier, W. R. Global glacial isostasy and the surface of the ice-age earth: The ice-5G (VM2) model and grace. Annual Review of Earth and Planetary Sciences 32, 111-149, doi:10.1146/annurev.earth.32.082503.144359 (2004).

49 Svendsen, J. I. et al. Late quaternary ice sheet history of northern Eurasia. Quaternary Science Reviews 23, 1229-1271, doi:10.1016/j.quascirev.2003.12.008 (2004).